5
The Whipple Bicycle

5.1 Background

The first substantial contribution to the theoretical bicycle literature was Whipple's seminal 1899 paper [2], which is arguably as contributory as anything written since (see Figure 5.1). This remarkable paper contains, for the first time, a set of nonlinear differential equations that describe the general motion of a bicycle and rider. Since the appropriate computing facilities were not available at the time, Whipple's general nonlinear equations could not be solved and consequently were not pursued beyond simply reporting them. Instead, Whipple studied a set of linear differential equations that correspond to small motions about a straight-running trim condition at a given constant speed. In the context of the nineteenth century, stability properties could be evaluated using the Routh criterion.

Whipple's model consists of two frames, namely the front frame and the rear frame, which are hinged together along an inclined steering-head assembly. The front and rear wheels are attached to the front and rear frames, respectively, and are free to rotate relative to them. The rider is described as an inert mass that is rigidly attached to the rear frame. The rear frame is free to roll and translate in the ground plane. Each wheel is assumed to be 'thin', and thus touches the ground at a single ground-contact point. The wheels, which are also assumed to be non-slipping, are modelled by holonomic constraints in the normal (vertical) direction and by nonholonomic constraints [41] in the longitudinal and lateral directions. From a mathematical perspective, the rolling disc (Section 2.10) and the bicycle wheels' contact dynamics are modelled in precisely the same way. There is no aerodynamic drag representation, no frame flexibility, and no suspension system—the rear frame is assumed to move at a constant speed. Since Whipple's linear straight-running model is fourth order, the corresponding characteristic polynomial is a quartic; see Figure 5.2.

Concurrent with Whipple's work, and apparently independently of it, Carvallo [54] derived the equations of motion for a free-steering bicycle linearized around a straight-running equilibrium condition. Klein and Sommerfeld [182] also derived equations of motion for a straight-running bicycle. Their slightly simplified model (as compared with that of Whipple) lumps the front wheel assembly mass into the front wheel. The main purpose of their study was to determine the effect of the gyroscopic moment due to the spinning front wheel on the machine's free-steering stability. They concluded that 'the gyroscopic effects, despite their smallness, are indispensable for the self-stability'. However, it was later pointed out that the analysis includes some algebra

Dynamics and Optimal Control of Road Vehicles. D. J. N. Limebeer and M. Massaro.

DOI: 10.1093/oso/9780198825715.001.0001

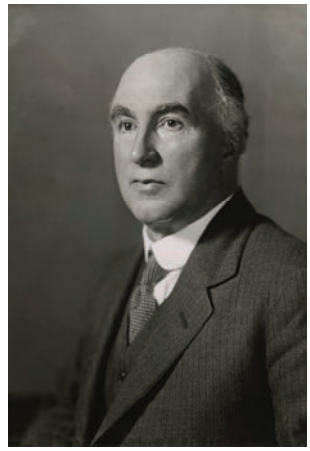

Figure 5.1: Francis John Welsh Whipple was born on March 17, 1876. He was educated at the Merchant Taylors' School and was subsequently admitted to Trinity College, Cambridge, in 1894. His university career was brilliant—he received his BA degree in mathematics in 1897 in the first class. Whipple received his MA in 1901 and an ScD in 1929. In 1899 he returned to the Merchant Taylors' School as a mathematics master; a post he held until 1914. Apart from his seminal work on bicycle dynamics, he made many other contributions to knowledge, including identities for generalized hypergeometric functions, several of which have subsequently become known as Whipple's identities and transformations. Reproduced with the permission of the National Portrait Galley, London.

mistakes, and the results reported are not valid for a general bicycle dataset [183].[1] While this moment does indeed stabilize the free-steering bicycle over a range of speeds, this effect is of only minor importance, because the rider can easily replace the stabilizing influence of the front wheel's gyroscopic precession with low-bandwidth rider control action [184].

An early attempt to introduce side-slipping and force-generating tyres into the bicycle literature appears in [185]. Other classical contributions to the theory of bicycle dynamics include [186] and [48]. The last of these references, in its original 1967 version, appears to contain the first analysis of the stability of the straight-running bicycle fitted with pneumatic tyres; several different tyre models are considered. Reviews of the bicycle literature from a dynamic modelling perspective can be found in [187]. The bicycle literature is comprehensively reviewed from a control theory perspective in [188], which also describes interesting bicycle-related experiments.

Some important and complementary applied work has been conducted in the context of bicycle dynamics. An attempt to build an unrideable bicycle (URB) is described in [184]. One of the URBs described had the gyroscopic moment of the front wheel

[1] Despite the calculation error, the conclusion is correct for the specific bicycle examined therein.

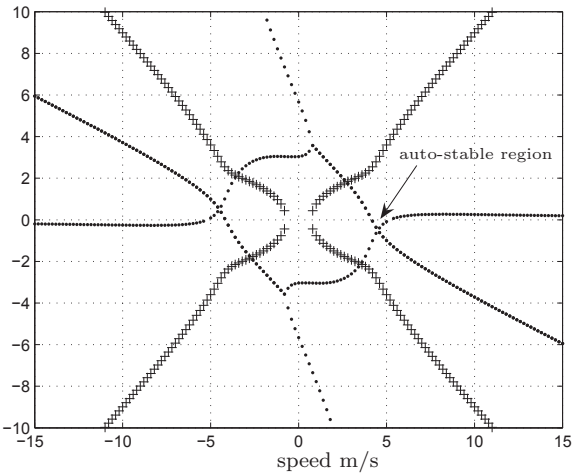

Figure 5.2: Stability properties of the 'Whipple bicycle'. Real (dots) and imaginary (crosses) parts of the eigenvalues of the straight-running Whipple bicycle model as functions of speed. Plot generated using equation (XXVIII) in [2], which was derived a century before the widespread availability of MATLAB!

cancelled by another which was counter-rotating. The cancellation of the front wheel's gyroscopic moment made little difference to the machine's apparent stability and handling qualities. It was also found that this riderless bicycle was unstable, an outcome that had been predicted theoretically in [182]. Three other URBs, described in [184], include various modifications to their steering geometry. These modifications include changes in the front wheel radius, and the magnitude and sign of the fork offset. Jones concluded that the castor trail is an important factor in the self-stability of single-track vehicles. However, it was later pointed out that the theoretical analysis therein reported is not valid for a general bicycle dataset [183].

After the results of [182] and [184], the gyroscopic effects and the trail have long been considered essential for the self-stability of bicycles (and single-track vehicles in general). A formal proof that this is not the case has been given recently in [169], where a self-stable bicycle with no gyroscopic effects and no castor trail has been analysed;[2] see Section 4.4.

Experimental investigations of bicycle dynamics have also been used in teaching [189].

[2] It is concluded that gyroscopic effects and castor trail, although not essential, are nevertheless beneficial to the stability of single-track vehicles of conventional design.

5.2 Bicycle model

As with Whipple's model, the bicycle model we consider here consists of two frames and two wheels. Figure 5.3 shows the axis systems and geometric layout of the bicycle model to be studied here The bicycle's rear frame assembly has a rigidly attached rider and a rear wheel that is free to rotate relative to the rear frame. The front frame, which comprises the front fork and handlebar assembly, has a front wheel that is free to rotate relative to the front frame. The front and rear frames are attached using a hinge that defines the steering axis. In the reference configuration, all four bodies are symmetric relative to the bicycle midplane. As with Whipple's model, the non-slipping road wheels are modelled by holonomic constraints in the normal (vertical) direction and by nonholonomic constraints in the longitudinal and lateral directions. There is no aerodynamic drag, no frame flexibility, no propulsion, and no rider control. The dimensions and mechanical properties of the benchmark model are taken from [187] and are presented in Table 5.1. All inertia parameters use the relevant body mass centres as the origins for body-fixed axes. The axis directions are then chosen to align with the inertial $Oxyz$ axes when the bicycle is in its nominal configuration, as shown in Figure 5.3. Products of inertia I_{Bxz}, I_{Hxz}, and so on are defined as $-\int\int xz\, m(x,z)dxdz$; see Section 2.7.

The wheels are modelled as axisymmetric, with each wheel making a point contact with the ground. The wheel-mass distributions need not be planar and so any positive inertias are allowed provided $I_{xx} = I_{zz}$ and $I_{xx} + I_{zz} \geq I_{yy}$; $I_{xx} + I_{zz} = I_{yy}$ in the

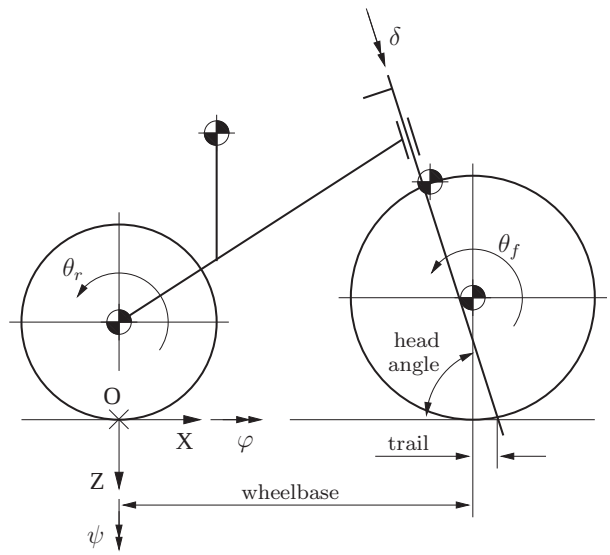

Figure 5.3: Whipple-type bicycle model with its degrees of freedom. The model comprises two frames pinned together along an inclined steering head. The rider is included as a rigidly attached part of the rear frame. Each wheel is assumed to contact the road at a single point.

Table 5.1 Bicycle parameters. The inertia matrices are referred to body-fixed axis systems that have their origins at the body's mass centre, and are aligned with the inertial reference frame $Oxyz$ when the machine is in its nominal configuration.

Parameters	**Symbol**	**Value**
Wheelbase	w	$1.02\,m$
Trail	t	$0.08\,m$
Head angle	α	$(2\pi)/5\,\text{rad}$
Steer axis tilt angle	λ	$\pi/10\,\text{rad}$
Gravity	g	$9.81\,m/s^2$
Rear wheel		
Radius	r_R	$0.3\,m$
Mass	m_R	$2\,kg$
Mass moments of inertia	$[I_{Rxx}, I_{Ryy}, I_{Rzz}]$	$[0.0603, 0.12, 0.0603]\,kg\,m^2$
Rear frame		
Position of centre of mass	$[x_B, y_B, z_B]$	$[0.3, 0.0, -0.9]\,m$
Mass	m_B	$85\,kg$
Mass moments of inertia	$\begin{bmatrix} I_{Bxx} & 0 & I_{Bxz} \\ & I_{Byy} & 0 \\ sym & & I_{Bzz} \end{bmatrix}$	$\begin{bmatrix} 9.2 & 0 & 2.4 \\ & 11 & 0 \\ sym & & 2.8 \end{bmatrix}\,kg\,m^2$
Front frame		
Position of centre of mass	$[x_H, y_H, z_H]$	$[0.9, 0.0, -0.7]\,m$
Mass	m_H	$4\,kg$
Mass moments of inertia	$\begin{bmatrix} I_{Hxx} & 0 & I_{Hxz} \\ & I_{Hyy} & 0 \\ sym & & I_{Hzz} \end{bmatrix}$	$\begin{bmatrix} 0.05892 & 0 & -0.00756 \\ & 0.06 & 0 \\ sym & & 0.00708 \end{bmatrix}\,kg\,m^2$
Front wheel		
Radius	r_F	$0.35\,m$
Mass	m_F	$3\,kg$
Mass moments of inertia	$[I_{Fxx}, I_{Fyy}, I_{Fzz}]$	$[0.1405, 0.28, 0.1405]\,kg\,m^2$

case of 'thin' planar wheels (equality follows from the perpendicular axis theorem; see Section 2.2.3).

This simple model is fully characterized by the twenty-five parameters listed in Table 5.1. Each parameter is defined in an upright reference configuration that has both wheels on a level ground plane and a zero steer angle. In the reference configuration the origin of the inertial coordinate system is at the rear-wheel ground-contact point O. We use the SAE vehicle dynamics sign convention that has the positive x-axis pointing forward, the positive z-axis pointing down and the positive y-axis pointing to the rider's right. Positive angles are defined in terms of a right-hand rule.

In the reference configuration the front-wheel ground-contact point is located at a distance w (the wheelbase) in front of the rear-wheel ground-contact point. The front-wheel ground-contact point trails a distance t behind the point where the steer axis intersects the ground. Although in standard bicycles and motorcycles the trail is also always positive, negative values of t can be contemplated. The steering head angle α is measured relative to the ground plane (in the machine's nominal configuration)—a steering head angle of $\pi/2$ would mean that the steering axis is vertical. The steer

axis tilt angle λ is measured from the negative z-axis and $\pi/2 = \alpha + \lambda$. The steer axis location is defined implicitly by the wheelbase w, trail t, and steering head angle.

5.2.1 Model features

Before we get immersed in the details of finding the bicycle's (linearized) equations of motion, there are a number of properties of the model that can be established using informal arguments.

Degrees of freedom. Let us begin by considering a bicycle floating in space. Under these conditions the main frame has six degrees of freedom—three translations and three rotations. The steering of the front frame introduces a seventh freedom, with two more freedoms associated with the rotations of the road wheels. At this point the accessible configuration space is nine-dimensional. Constraining the rear-wheel ground-contact point to the x–y plane removes the z-dimensional translational freedom of the main frame, thereby reducing the configuration space to eight dimensions. One more freedom is removed once the front-wheel ground-contact point is constrained to the ground plane. This constraint also introduces a closed kinematic loop that constrains the main body's pitch freedom. A kinematic analysis of the type to be given in Section 7.7.1 shows that the main-body pitch angle χ can be expressed in terms of the vehicle's roll and steer angles (φ and δ respectively) as follows

$$\chi = \chi_0 - \frac{t_n}{w}\delta \tan\varphi \tag{5.1}$$

in the case that the pitch and steer angle variations are 'small'; χ_0 is the main-body pitch angle in the nominal configuration. If the roll angle variations are also assumed 'small', the main-body pitch angle is constant to first order.

Prior to considering the nonholonomic constraints associated with non-slipping wheels, the accessible configuration space is seven-dimensional. Since the four nonholonomic constraints associated with the non-slipping road wheels are velocity constraints, they do not reduce further the dimension of the accessible configuration space. By invoking manoeuvres akin to vehicle parking, one can still access the whole of the ground plane, arbitrary yaw angles, and arbitrary road–wheel position angles. The bicycle's accessible configuration space is seven-dimensional.

Summarizing, the first two freedoms (x_R, y_R) specify the rear-wheel ground-contact point in an inertial coordinate system. The orientation of the main frame is defined relative to a global coordinate system in terms of a sequence of three rotations. The third and fourth freedoms are the yaw angle ψ and the roll angle φ—the pitch angle χ is constrained by a closed kinematic loop generated by the wheel ground-contact constraints. The front frame is free to rotate relative to the rear frame through the steer angle δ—this gives five degrees of freedom. Finally, there are two wheel rotation angles θ_R and θ_F. The bicycle configuration is therefore defined in terms of the seven (position) variables x_R, y_R, ψ, φ, δ, θ_R, and θ_F.

Velocity freedoms. As was explained in some detail in the context of the rolling disc (Section 2.10), there are four nonholonomic constraints associated with the road wheels

(two for each wheel). This reduces the number of velocity freedoms by four. The resulting three-dimensional, kinematically accessible velocity space can be characterized in terms of $\dot{\varphi}$, $\dot{\delta}$, and $\dot{\theta}_R$. The remaining four velocities $\dot{x}_R$, $\dot{y}_R$, $\dot{\psi}$, and $\dot{\theta}_F$ are made dependent by the rolling contact constraints.

State variables. Seven position variables and three velocity variables are necessary to describe the Whipple bicycle. In some models this number can be reduced further by removing the ignorable/cyclic coordinates (Section 2.3). Under the assumption of axisymmetric wheels, θ_R and θ_F can be treated as cyclic. The vehicle's dynamics are invariant under translation and rotation on the road plane and x_R, y_R, and ψ are cyclic too. The remaining position variables are φ and δ, together with three velocity variables $\dot{x}_R$, $\dot{\varphi}$, and $\dot{\delta}$. The final set of state variables is thus

$$[\dot{x}_R, \dot{\varphi}, \dot{\delta}, \varphi, \delta]^T. \tag{5.2}$$

It is often convenient to replace the longitudinal velocity $\dot{x}_R$ of the rear contact point with its absolute velocity $u = \dot{x}_R / \cos\psi$. Consequently the state vector is

$$[u, \dot{\varphi}, \dot{\delta}, \varphi, \delta]^T. \tag{5.3}$$

In constant-speed models the state-vector reduces even further to

$$[\dot{\varphi}, \dot{\delta}, \varphi, \delta]^T. \tag{5.4}$$

Energy conservation. In the analysis of the Čhaplygin sleigh given in Section 2.8, it was observed that in the nonlinear model any initial misalignment in the yaw angle would produce yaw oscillations that would die away until the sleigh was again aligned with the velocity vector. Since this is a conservative system, the (kinetic) energy associated with the yaw oscillations is transferred into the kinetic energy of forward motion; see Figure 2.14. In the linear model speed and yaw motions are decoupled and consequently the speed does not change, no energy transfer takes place, and the yaw energy is dissipated. Precisely the same phenomena occur in the Whipple bicycle. First, linearization ensures that the bicycle's speed remains unaltered, and any energy associated with oscillatory behaviour is simply dissipated (in the stable speed range). In contrast, if the nonlinear Whipple bicycle is running at some initial speed, with non-zero initial conditions in the roll and/or steer freedoms, then the associated oscillations will die away, transferring the associated energy into the forward velocity. This behaviour is seen in Figure 5.4, where there is an initial disturbance in the vehicle's roll angle velocity. This produces asymptotically stable roll and steer responses that transfer their energy into the forward speed, which increases by approximately 0.07 m/s in the given example.

Lateral dynamics decoupling. Consider the equations of motion describing the bicycle's small-perturbation dynamics relative to constant-speed straight running. In this case initial values of the vehicle's velocity, roll angle, and steer angle will evolve with time according to

$$\begin{bmatrix} u(t_f) \\ \varphi(t_f) \\ \delta(t_f) \end{bmatrix} = \begin{bmatrix} \Phi_{11}(t_f - t_0) & \Phi_{12}(t_f - t_0) & \Phi_{13}(t_f - t_0) \\ \Phi_{21}(t_f - t_0) & \Phi_{22}(t_f - t_0) & \Phi_{23}(t_f - t_0) \\ \Phi_{31}(t_f - t_0) & \Phi_{32}(t_f - t_0) & \Phi_{33}(t_f - t_0) \end{bmatrix} \begin{bmatrix} u(t_0) \\ \varphi(t_0) \\ \delta(t_0) \end{bmatrix},$$

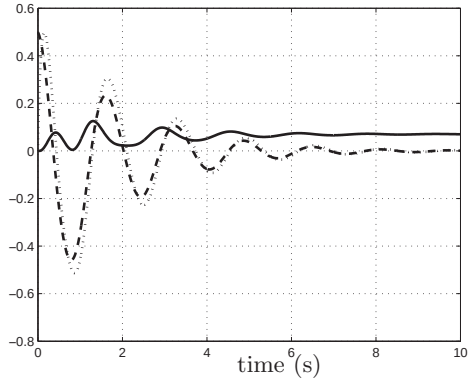

Figure 5.4: Nonlinear energy transfer properties of the straight-running Whipple bicycle. The free-rolling bicycle has an initial velocity of 4.5 m/s, which is in the stable speed range illustrated in Figure 5.5. There is an initial roll velocity is 0.5 rad/s. Plotted are the roll velocity (dashed) and steer angle velocity (dotted), and speed variation about its initial value of 4.5 m/s (solid).

in which $u(t_0)$, $\varphi(t_0)$, and $\delta(t_0)$ are initial values of the bicycle's speed, roll angle, and steering angle respectively. The matrix $\Phi(t_f - t_0)$ is the transition matrix associated with the straight-running linearized equations of motion. Since these equations are linear, negating the initial conditions will negate the final solution.

Consider the initial condition $\begin{bmatrix} 0 & \epsilon & 0 \end{bmatrix}$, which represents a perturbation to the machine's roll angle. This will cause the machine to either speed up or slow down. Either way, the same speed variation will occur in response to the condition $\begin{bmatrix} 0 & -\epsilon & 0 \end{bmatrix}$. It therefore follows that $\Phi_{12}(t_f - t_0) = 0$. It follows from a parallel argument relating to an initial steering angle perturbation $\begin{bmatrix} 0 & 0 & \epsilon \end{bmatrix}$ that $\Phi_{13}(t_f - t_0) = 0$. Now consider a small forward speed variation $\begin{bmatrix} \epsilon & 0 & 0 \end{bmatrix}$. The roll and steering angle will respond in some unspecified manner. Intuitively one would expect this same response from a negated version of this speed variation and so $\Phi_{21}(t_f - t_0) = 0$ and $\Phi_{31}(t_f - t_0) = 0$ must hold. If we now consider the unperturbed nonlinear equations of motion with initial speed $u(t_0)$, conservation of energy dictates that $u(t_f) = u(t_0)$ for all t_f. If one then applies a small initial speed variation, then this same speed variation will persist for all time and so $\Phi_{11}(t_f - t_0) = 1$, giving

$$\Phi(t_f - t_0) = \begin{bmatrix} 1 & 0 & 0 \\ 0 & \Phi_{22}(t_f - t_0) & \Phi_{23}(t_f - t_0) \\ 0 & \Phi_{32}(t_f - t_0) & \Phi_{33}(t_f - t_0) \end{bmatrix} \tag{5.5}$$

for all $t_f - t_0$.

These informal arguments demonstrate that to first order the in-plane and lateral dynamics are decoupled. Thus a bicycle with a constrained forward speed will have the same linearized equations of motion as one in which the forward speed is a free variable.

5.3 Linear in-plane dynamics

We begin by considering the in-plane dynamics of a bicycle in which the steering is locked and with the machine constrained in roll. Under these conditions a (rear-wheel) drive torque T_R is required to accelerate the machine's mass as well as spin up the angular momentum of both wheels. The assumed constraints preclude steer and roll angle contributions to the longitudinal dynamics. A force balance in the direction of motion and a moment balance around the wheel spin axes give the the following equations of motion:

$$m_T\dot{u} = F_{x_R} + F_{x_F} \tag{5.6}$$

$$I_{Ryy}\ddot{\theta}_R = F_{x_R}r_R + T_R \tag{5.7}$$

$$I_{Fyy}\ddot{\theta}_F = F_{x_F}r_F, \tag{5.8}$$

in which T_R is the drive/braking torque. Substitution of the expressions for F_{x_R} and F_{x_F}, derived in (5.7) and (5.8), into (5.6) gives

$$m_T\dot{v} = I_{Ryy}\frac{\ddot{\theta}_R}{r_R} - \frac{T_R}{r_R} + I_{Fyy}\frac{\ddot{\theta}_F}{r_F}. \tag{5.9}$$

Enforcing the no-slip conditions gives $\dot{u} = -\ddot{\theta}_R r_R$ and $\dot{u} = -\ddot{\theta}_F r_F$, which implies that $\ddot{\theta}_F = \ddot{\theta}_R r_R/r_F$ and

$$\left(r_R^2 m_T + I_{Ryy} + \left(\frac{r_R}{r_F}\right)^2 I_{Fyy}\right)\ddot{\theta}_R = T_R, \tag{5.10}$$

in which m_T is the total vehicle mass given by

$$m_T = m_R + m_F + m_B + m_H. \tag{5.11}$$

In the case that $T_R = 0$, the machine speed is constant and given by $u = -\dot{\theta}_R r_R$. It follows from (5.6) that the rear tyre longitudinal force F_{x_R} (assuming $F_{x_F} = 0$) must accelerate the total mass m_T of the vehicle, while (5.10) shows that the rear-wheel torque T_R must accelerate the total apparent mass of the vehicle that includes the inertial terms I_{Ryy}/r_R^2 and I_{Fyy}/r_F^2.

If we now consider small perturbations about the trim condition described in (5.10), and recollect from (5.5) that there is no cross-coupling between the longitudinal and lateral dynamics (to first order), we conclude that (5.10) also serves as a linear first-order small-perturbation equation for the vehicle's longitudinal dynamics. As with Čhaplygin's sleigh, the linearization process destroys the system's conservation properties and removes the cross-coupling between the longitudinal and lateral dynamics; in the non-linear model the energy transfer between the longitudinal and lateral dynamics occurs via higher-order terms.

5.4 Linear out-of-plane dynamics

The treatment given here follows closely that given in [187]. Without loss of generality we can assume that the bicycle is rolling freely in a forward direction along the

positive x-axis of a global inertial coordinate system. We will suppose also that the vehicle has been perturbed from a straight-running equilibrium—the perturbation is assumed 'small' so that linear behaviour can be assumed. The linearized equation of motion for the longitudinal dynamics has already been presented in (5.10). The external influences of importance include gravitational forces that act in the direction of the (positive) inertial z-axis, reaction forces at the two wheel ground-contact points, forces of constraint that act in the inertial $x - y$ plane and which correspond to non-slip rolling, a propulsion torque T_R that acts on the rear wheel, a steering torque T_{HB} that acts on the front frame and reacts on the rear frame, and a roll torque T_B that acts on the rear frame. The equations of motion will be derived using standard Newton–Euler-type angular momentum balance arguments; see Section 2.2 and (2.11).

5.4.1 Intermediate variables

Following [187] we will now introduce a number of intermediate variables that will be used in the sequel. Quantities associated with the four rigid bodies will be labelled as follows: a subscript 'R' will be used for parameters or variables relating to the rear wheel, a subscript 'B' will be used for the rear frame, a subscript 'F' will be used for the front wheel, and a subscript 'A' will be used for parameters or variables relating to the front frame assembly.

The combined mass of the bicycle is given in (5.11). When the bicycle is in its nominal configuration, the whole-machine mass centre is located at:

$$\begin{aligned} x_T &= (x_B m_B + x_H m_H + w m_F)/m_T \\ z_T &= (-r_R m_R + z_B m_B + z_H m_H - r_F m_F)/m_T. \end{aligned}$$

Note that z_T is negative as are each of the coordinates of the individual mass centres.

The whole-machine moments and products of inertia are given next. These will be computed relative to the rear-wheel ground-contact point and along the inertial axes:

$$\begin{aligned} I_{Txx} &= I_{Rxx} + I_{Bxx} + I_{Hxx} + I_{Fxx} + m_R r_R^2 + m_B z_B^2 + m_H z_H^2 + m_F r_F^2 \\ I_{Txz} &= I_{Bxz} + I_{Hxz} - m_B x_B z_B - m_H x_H z_H + m_F w r_F \\ I_{Tzz} &= I_{Rzz} + I_{Bzz} + I_{Hxzz} + I_{Fzz} + m_B x_B^2 + m_H x_H^2 + m_F w^2. \end{aligned}$$

A parallel set of calculations can be carried out for the front frame assembly. The mass of the front frame assembly is:

$$m_A = m_H + m_F, \tag{5.12}$$

while the front assembly mass centre is given by

$$\begin{aligned} x_A &= (x_H m_H + w m_F)/m_A; \\ z_A &= (z_H m_H - r_F m_F)/m_A. \end{aligned}$$

The front assembly moments and products of inertia (with respect to the mass centre) are given next,

$$I_{Axx} = I_{Hxx} + I_{Fxx} + m_H(z_H - z_A)^2 + m_F(r_F + z_A)^2;$$
$$I_{Axz} = I_{Hxz} - m_H(x_H - x_A)(z_H - z_A) + m_F(w - x_A)(r_F + z_A);$$
$$I_{Azz} = I_{Hzz} + I_{Fzz} + m_H(x_H - x_A)^2 + m_F(w + x_A)^2.$$

A number of other quantities relating to the front frame geometry are also required. To begin, we will need the perpendicular distance between the front frame mass centre and the steering axis, which follows by simple planar geometry.[3] One of the equations of motion to follow comes from taking moments around the steering axis; we will therefore need the moment of inertia of the front assembly around this axis, which is computed by application of (2.14) with $\mathcal{R} = \mathcal{R}(\boldsymbol{e}_y, \lambda)$ and (2.13) with $\boldsymbol{r} = [u_A, 0, 0]^T$:

$$I_{A\lambda\lambda} = m_A u_A^2 + I_{Axx}\sin^2\lambda + 2I_{Axz}\sin\lambda\cos\lambda + I_{Azz}\cos^2\lambda. \tag{5.14}$$

We will also require product-of-inertia terms associated with the moments generated around the inertial x- and z-axes by steering angular accelerations:

$$I_{A\lambda x} = -m_A u_A z_A + I_{Axx}\sin\lambda + I_{Axz}\cos\lambda$$
$$I_{A\lambda z} = m_A u_A x_A + I_{Axz}\sin\lambda + I_{Azz}\cos\lambda.$$

The expressions for these inertia terms can be obtained from (2.11) by taking moments around O considering (small) steer perturbations δ

$$\begin{bmatrix} \ddot{\delta}\, I_{A\lambda x} \\ 0 \\ \ddot{\delta}\, I_{A\lambda z} \end{bmatrix} = \frac{d\boldsymbol{H}_O}{dt} \qquad \boldsymbol{H}_O = \begin{bmatrix} I_{Axx} & 0 & I_{Axz} \\ 0 & I_{Ayy} & 0 \\ I_{Axz} & 0 & I_{Azz} \end{bmatrix} \begin{bmatrix} \dot{\delta}\sin\lambda \\ 0 \\ \dot{\delta}\cos\lambda \end{bmatrix} + \boldsymbol{r}_{OA} \times \boldsymbol{P}_A, \tag{5.15}$$

where

$$\boldsymbol{r}_{OA} = \begin{bmatrix} x_A \\ u_A\delta \\ z_A \end{bmatrix} \qquad \boldsymbol{P}_A = \begin{bmatrix} 0 \\ m_A u_A \dot{\delta} \\ 0 \end{bmatrix}. \tag{5.16}$$

[3] Consider the similar triangles in the figure

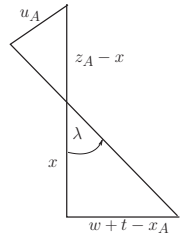

It follows that

$$\tan\lambda = \frac{w + t - x_A}{x} \qquad \sin\lambda = \frac{u_A}{z_A - x},$$

in which x is unknown. Equation (5.13) follows by eliminating x from the above equations (z_A is assumed negative),

$$u_A = (x_A - w - t)\cos\lambda - z_A\sin\lambda. \tag{5.13}$$

The reaction force at the front-wheel ground-contact point will appear in the moment calculations given in the sequel. The sum of the front- and rear-wheel reaction forces is given by

$$N_F + N_R = gm_T.$$

When the bicycle is in its nominal configuration we also have

$$N_F = gm_T x_T / w \tag{5.17}$$

and so

$$N_R = gm_T(1 - \frac{x_T}{w}). \tag{5.18}$$

The rear- and front-wheel angular momenta along their y-axes, divided by the forward speed, form the gyrostatic coefficients:

$$S_R = \frac{I_{Ryy}}{r_R} \qquad S_F = \frac{I_{Fyy}}{r_F} \qquad S_T = S_R + S_F. \tag{5.19}$$

We conclude with two intermediate variables that appear in relation to the steering geometry:

$$\mu = \frac{t\cos\lambda}{w} \quad \text{and} \quad S_A = m_A u_A + \mu m_T x_T.$$

5.4.2 Equations of motion

Using (2.9), the moment balance (2.11) can be rewritten as

$$\sum_{i\,\in\,\text{bodies}} [\mathbf{r}_i \times \mathbf{a}_i m_i + I_i \dot{\boldsymbol{\omega}}_i + \boldsymbol{\omega}_i \times (I_i \boldsymbol{\omega}_i)] = \sum_{j\,\in\,\text{forces}} [\mathbf{r}_j \times \mathbf{F}_j] \tag{5.20}$$

in the case of an instantaneously stationary pivot point. The vectors $\mathbf{r}_i$ and $\mathbf{r}_j$ give the positions of the body mass centres and applied forces respectively, $\boldsymbol{\omega}_i$ are the angular velocities,[4] and $\boldsymbol{a}_i$ is the acceleration of the mass centres. Right-hand-side forces include gravitational forces and tyre forces, with normal loads given by (5.17) and (5.18) and lateral forces unknown. Three equations of motion will be computed: roll balance, yaw balance and steer balance. These equations will eventually be reduced to two, after elimination of the front-wheel lateral force and enforcement of the nonholonomic constraints.

The first equation of motion comes from a momentum balance around an axis $\boldsymbol{u}$ in the ground plane that is instantaneously aligned with the line of intersection between the rear frame and the ground plane. Note that the rear-wheel ground-contact point

[4] The angular velocities related to the whole bike ω_T, front assembly ω_A, rear wheel ω_R, and front wheel ω_F, expressed in a frame yawed with the bicycle, are (see Section 2.5)

$$\boldsymbol{\omega}_T = \begin{bmatrix} \dot{\phi} \\ 0 \\ \dot{\psi} \end{bmatrix} \quad \boldsymbol{\omega}_A = \begin{bmatrix} \dot{\phi} + \dot{\delta}\sin\lambda \\ 0 \\ \dot{\psi} + \dot{\delta}\cos\lambda \end{bmatrix} \quad \boldsymbol{\omega}_R = \begin{bmatrix} \dot{\phi} \\ -u/r_R \\ \dot{\psi} - \phi u/r_R \end{bmatrix} \quad \boldsymbol{\omega}_F = \begin{bmatrix} \dot{\phi} + \dot{\delta}\sin\lambda + \delta\frac{u}{r_F}\cos\lambda \\ -u/r_F \\ \dot{\psi} + \dot{\delta}\cos\lambda - \phi u/r_F - \delta\frac{u}{r_F}\sin\lambda \end{bmatrix}.$$

falls on this line, but in general the front-wheel ground-contact point will not. In conformity with (5.20), and ignoring temporarily the rolling constraints, we obtain:

$$\begin{aligned} &-m_T\ddot{y}_R z_T + I_{Txx}\ddot{\varphi} + I_{Txz}\ddot{\psi} + I_{A\lambda x}\ddot{\delta} + u\dot{\psi}S_T + u\dot{\delta}S_F\cos\lambda \\ &= T_B - gm_T z_T\varphi + gu_A m_A\delta + g\mu x_T m_T\delta \\ &= T_B - gm_T z_T\varphi + gS_A\delta. \end{aligned} \tag{5.21}$$

The last two terms on the left-hand side are yaw- and steer-related gyroscopic effects. The terms on the right include an external roll moment T_B (e.g. a wind gust), a roll-related gravitational term, a steer-related gravitational term, and a term related to the reaction force at the front-wheel ground-contact point.[5]

The next equation comes from an angular momentum balance for the whole machine about an axis parallel to the inertial z-axis and that passes through the rear-wheel ground-contact point:

$$m_T x_T\ddot{y}_R + I_{Txz}\ddot{\varphi} + I_{Tzz}\ddot{\psi} + I_{A\lambda z}\ddot{\delta} - u\dot{\varphi}S_T - u\dot{\delta}S_F\sin\lambda = wF_{y_F}. \tag{5.22}$$

Again, the last two terms on the left-hand side are yaw- and steer-related gyroscopic terms. The only external force is the lateral front-wheel ground-contact reaction force F_{y_F}, which acts at the front-wheel ground-contact point. This force acts in the ground plane and is perpendicular to the line of intersection between the ground plane and the plane of symmetry of the front wheel.

The last equation comes from an angular momentum balance for the steering axis.

$$\begin{aligned} m_A u_A\ddot{y}_R + I_{A\lambda x}\ddot{\varphi} + I_{A\lambda z}\ddot{\psi} + I_{A\lambda\lambda}\ddot{\delta} + uS_F(\dot{\psi}\sin\lambda - \dot{\varphi}\cos\lambda) \\ = T_{HB} - tF_{y_F}\cos\lambda + g(\varphi + \delta\sin\lambda)S_A. \end{aligned} \tag{5.23}$$

The right-hand side of this equation contains forcing terms from the steering moment T_{HB}, the front-wheel ground-reaction force, and steering-geometry-related roll

[5] The roll-related gravitational term is easy to visualize. The other terms are a little more subtle, as can be appreciated by studying the diagram of the upright bicycle with its steering assembly steered to the right.

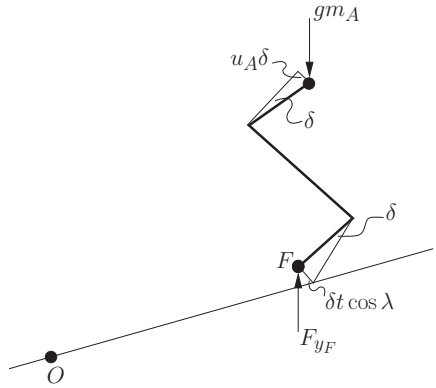

and steer terms. As we are only interested in first-order contributions, we consider separately the gravitational roll moments,[6] and then those due to steering.[7]

In order to obtain a final set of equations that describe the bicycle's dynamics for small perturbations from straight running we need to eliminate the front-wheel ground-contact force F_{y_F} from (5.22) and (5.23), and then recognize the nonholonomic rolling constraints associated with the two road wheels. In essence, the rolling constraints allow the lateral position and its derivatives, and the yaw angle and its derivatives to be expressed in terms of the steer angle. As explained earlier, the cyclic coordinates can then be recovered by integrating the nonholonomic rolling constraints. Assuming that the bicycle is travelling along the positive x-axis, the lateral velocity of the rear-wheel ground-contact point is

$$\dot{y}_R = u\psi \tag{5.24}$$

for small values of yaw angle. The lateral velocity of the front-wheel ground contact point can be recovered from the front wheel position. It follows from the figure in the

[6] Consider the rolled machine in which the steering assembly is in its neutral (straight-ahead) position. In combination, the gravitational and front-wheel reaction forces produce a moment $gS_A\varphi$.

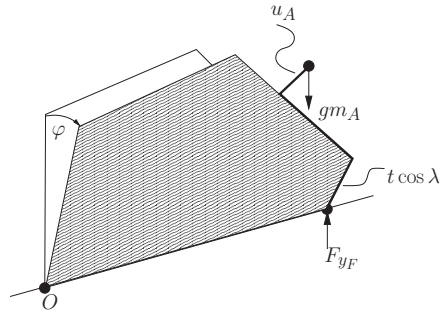

[7] Consider in the figure the upright steered machine. The component of the gravitational force acting on the front frame assembly mass centre that is perpendicular to the steering axis produces moment $gm_A u_A \sin\lambda$, while the component of the front-wheel reaction force acting perpendicular to the steering axis produces a moment $tF_{y_F}\sin\lambda\cos\lambda$.

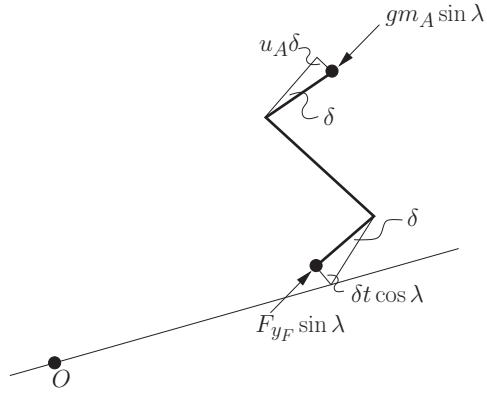

footnote on page 207 that the front wheel position is

$$y_F = y_R + w\psi - t\cos\lambda\delta. \tag{5.25}$$

For the front wheel, the body-fixed coordinate system is rotated with respect to the global z-axis by an amount $\psi + \delta\cos\lambda$. The lateral velocity of the front wheel is therefore given by

$$\frac{dy_F}{dt} = u(\psi + \delta\cos\lambda) \;\Rightarrow\; \dot{\psi} = \frac{u\delta + t\dot{\delta}}{w}\cos\lambda, \tag{5.26}$$

which gives

$$\ddot{\psi} = \frac{u\dot{\delta} + t\ddot{\delta}}{w}\cos\lambda, \tag{5.27}$$

$$\ddot{y}_R = \frac{u^2\delta + vt\dot{\delta}}{w}\cos\lambda. \tag{5.28}$$

The final roll equation comes from (5.21), once $\ddot{y}_R$, $\ddot{\psi}$, and $\dot{\psi}$ have been eliminated using (5.26), (5.27), and (5.28) respectively. The steer equation comes from eliminating the front tyre side force F_{y_F} from (5.22) and (5.23) (which corresponds to using μ(5.22)+(5.23)), followed by the removal of $\ddot{y}_R$, $\ddot{\psi}$, and $\dot{\psi}$ as before. The resulting equations can be written in the form

$$M\ddot{\boldsymbol{q}} + uC\dot{\boldsymbol{q}} + (gK_0 + u^2K_2)\boldsymbol{q} = \begin{bmatrix} T_B \\ T_{HB} \end{bmatrix}, \tag{5.29}$$

where

$$\boldsymbol{q} = \begin{bmatrix} \varphi \\ \delta \end{bmatrix}.$$

The entries of the mass, damping, and stiffness matrices are given by

$$\begin{aligned}
M_{11} &= I_{Txx} \\
M_{12} &= I_{A\lambda x} + \mu I_{Txz} \\
M_{21} &= M_{12} \\
M_{22} &= I_{A\lambda\lambda} + 2\mu I_{A\lambda z} + \mu^2 I_{Tzz},
\end{aligned}$$

$$\begin{aligned}
C_{11} &= 0 \\
C_{12} &= \mu S_T + S_F\cos\lambda + \frac{I_{Txz}}{w}\cos\lambda - \mu m_T z_T \\
C_{21} &= -(\mu S_T + S_F\cos\lambda) \\
C_{22} &= \frac{I_{A\lambda z}}{w}\cos\lambda + \mu\left(S_A + \frac{I_{Tzz}}{w}\cos\lambda\right),
\end{aligned}$$

$$\begin{aligned}
K_{011} &= m_T z_T \\
K_{012} &= -S_A \\
K_{021} &= K_{012} \\
K_{022} &= -S_A\sin\lambda,
\end{aligned}$$

and

$$\begin{aligned} K_{211} &= 0 \\ K_{212} &= \frac{S_T - m_T z_T}{w} \cos\lambda \\ K_{221} &= 0 \\ K_{222} &= \frac{S_A + S_F \sin\lambda}{w} \cos\lambda \end{aligned}$$

respectively.

The cyclic coordinates, which determine the bicycle's position and orientation, can be recovered a posteriori by integrating the relevant nonholonomic constraint equations. Since these equations do not appear in (5.29), they need not conform to the small-perturbation assumption. The vehicle's yaw can be found by integrating (5.26). After that, the machine's global position can be found by integrating

$$\dot{x}_P = u\cos\psi \qquad \dot{y}_P = u\sin\psi, \tag{5.30}$$

which, unlike (5.24), do not assume small yaw angles.

5.4.3 Modal analysis

In order to study the modal behaviour of the Whipple bicycle as described in equation (5.29), we begin by introducing the matrix-valued polynomial

$$P(s,v) = s^2 M + suC + (u^2 K_2 + gK_0), \tag{5.31}$$

which is quadratic in both the forward speed u and in the Laplace variable s. The associated transfer function equation is

$$\begin{bmatrix} P_{11}(s) & P_{12}(s,u) \\ P_{21}(s,u) & P_{22}(s,u) \end{bmatrix} \begin{bmatrix} \varphi(s) \\ \delta(s) \end{bmatrix} = \begin{bmatrix} T_B(s) \\ T_{HB}(s) \end{bmatrix}, \tag{5.32}$$

where notably P_{11} is independent of u. When studying stability, the roots of the speed-dependent quartic equation

$$\det(P(s,u)) = 0 \tag{5.33}$$

must be analysed using numerical methods.[8]

Figure 5.5 shows the loci of the roots of (5.33) as functions of the forward speed. As with the simple inverted pendulum that has eigenvalues at $\pm\lambda_i$, a number of symmetries exist in the Whipple bicycle spectrum. At zero speed, if λ_i is an eigenvalue

[8] A convenient approach is to cast (5.29) in the state-space form $\dot{\boldsymbol{x}} = A\boldsymbol{x} + B\boldsymbol{u}$ and compute the eigenvalues of the A matrix given by

$$A = \begin{bmatrix} 0 & I \\ -M^{-1}(u^2 K_2 + gK_0) & -M^{-1}uC \end{bmatrix}. \tag{5.34}$$

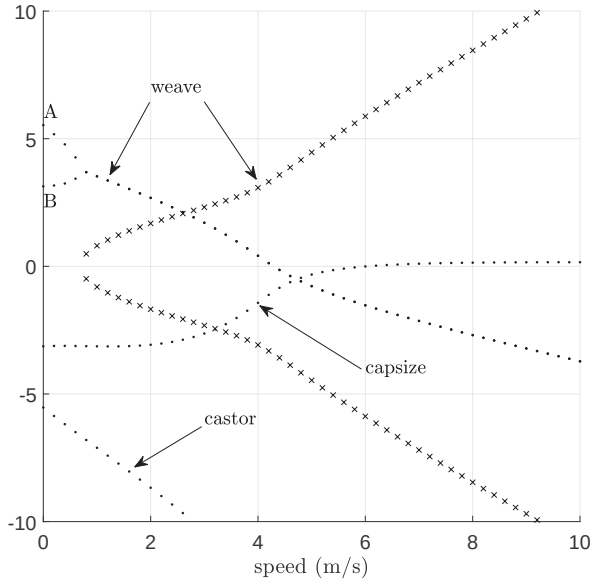

Figure 5.5: Whipple bicycle straight-running stability properties. Real and imaginary parts of the eigenvalues of the straight-running bicycle model as functions of speed. The dotted lines correspond to the real part of the eigenvalues and the crosses show the imaginary parts for the weave mode. The weave-mode eigenvalue stabilizes at $u_w = 4.3\,\mathrm{m/s}$, while the capsize mode becomes unstable at $u_c = 6.0\,\mathrm{m/s}$, giving the stable speed range $u_c \geq u \geq u_w$.

then so is $-\lambda_i$. It is also evident from (5.31) that if λ_i is an eigenvalue at speed u, then $-\lambda_i$ is an eigenvalue at speed $-u$. We will now examine each of the eigenvalues in a little more detail. The numerical values reported herein are obtained using the dataset in Table 5.1.

The Whipple bicycle has two important modes, namely, weave and capsize. The weave mode begins at zero speed with the two unstable eigenvalues marked A and B in Figure 5.5; these modes are the steer-capsize and body-capsize modes respectively. The eigenvector corresponding to the A-mode eigenvalue is steer dominated (hence the name steer-capsize) and has a steer-to-roll ratio of -36.9; the negative sign means that as the bicycle rolls (to the right, say), the steering rotates anti-clockwise as viewed from above. This shows that the motion associated with the A-mode is dominated by the front frame diverging towards full lock as the machine rolls over under gravity. Since real tyres make distributed contact with the ground, a real bicycle cannot be expected to behave in exact accordance with this prediction. The eigenvector components corresponding to the B-mode (body-capsize) eigenvalue has a steer-to-roll ratio of -0.55. The associated motion involves the rear frame toppling over, or capsizing, like an unconstrained inverted pendulum (to the right say), while the steering assembly rotates relative to the rear frame to the left. The term 'capsize' is used in three different

contexts. The static and very low-speed capsizing of the bicycle front steered assembly and the main frame are associated with the points A and B, respectively, and the associated nearby loci; see Figure 5.5. The locus marked capsize in Figure 5.5 is associated with the higher-speed toppling and lateral translation of the vehicle. This mode crosses the stability boundary and becomes unstable when the matrix $u^2K_2 + gK_0$ in (5.29) and (5.34) is singular.[9]

As the machine speed builds up from zero, the unstable (real) steer-capsize and body-capsize modes combine at approximately 0.6 m/s to produce the oscillatory fish-tailing weave mode. The Whipple bicycle model predicts that the weave mode frequency is approximately proportional to speed for speeds above 0.6 m/s. In contrast, the capsize mode is a non-oscillatory motion, which when unstable, corresponds to the unsteered bicycle slowly toppling over at speeds above 6.0 m/s. From the perspective of bicycle riders and designers, this mode is only of minor consequence, since it is either an artefact of the model, or is easily stabilized by the rider. In practice, the capsize mode can also be stabilized using appropriately phased rider body motions, as is evident from hands-free riding. There is a third well damped mode called the castor mode, which describes the self aligning of the steering system—like the straightening of a supermarket trolley castor wheel.

In a measurement program an instrumented bicycle was used in [190] to validate the Whipple bicycle model described in [2] and [187]. The measurement data show close agreement with the model in the 3–6 m/s speed range; the weave mode frequency and damping agreement are noteworthy. The transition of the weave mode from the stable to the unstable speed ranges is also accurately predicted by the Whipple model. These measurements lend credibility to the idea that tyre and frame compliance effects can be neglected for benign manoeuvring in the 0–6 m/s range.

5.4.4 Gyroscopic influences

Gyroscopic precession is a favourite topic of conversation in bar-room discussions amongst motorcyclists. While it is not surprising that lay people have difficulty understanding these effects, inconsistencies also appear in the technical literature on single-track vehicle behaviour, as already alluded to in Section 5.1.

The experimental evidence is a good place to begin the process of understanding gyroscopic influences. Experimental bicycles whose gyroscopic influences are cancelled through the inclusion of counter-rotating wheels have been designed and built [184]. Other machines have had their gyroscopic influences exaggerated through the use of a high-moment-of-inertia front wheel [188]. In both cases the bicycles were found to be easily ridable. As with the stabilization of the capsize mode by the rider, the precession-cancelled bicycle appears to represent little more than a simple low-bandwidth challenge to the rider. As noted in [184], in connection with his precession-cancelled bicycle, '... Its "feel" was a bit strange, a fact I attributed to the increased moment of inertia about the front forks, but it did not tax my (average) riding skill even at low speed...'. When trying to ride this particular bicycle without hands, however, the

[9] The matrix in (5.29) has a zero eigenvalue when $u^2K_2 + gK_0$ is singular.

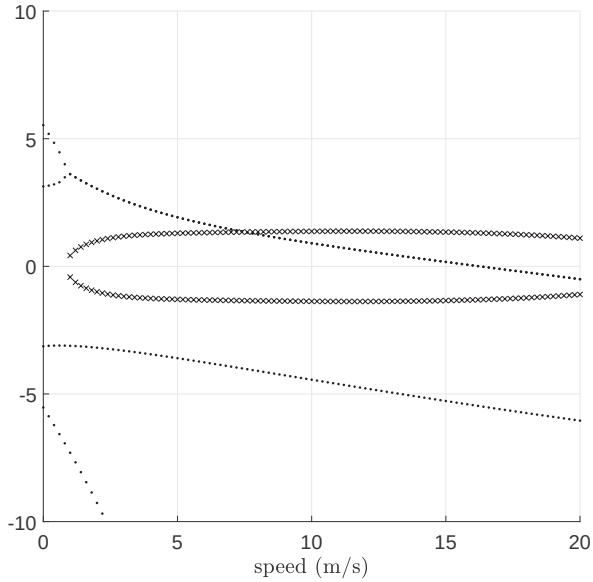

Figure 5.6: Gyroscopic stability properties. Real and imaginary parts of the eigenvalues of the straight-running Whipple bicycle with the gyroscopic moment associated with the front road wheel removed (by setting $I_{Fyy} = 0$). The dotted lines correspond to the real parts of the eigenvalues, while the crosses show the imaginary parts.

rider could only just keep it upright, because the vehicle seemed to lack balance and responsiveness.

In their theoretical work Klein and Sommerfeld [182] studied a Whipple-like quartic characteristic equation using the Routh criterion. While the Whipple bicycle model has a stable range of speeds, which Klein and Sommerfeld called the interval of auto-stability, this model with the spin inertia of the front wheel set to zero is unstable up to a speed of 16.2 m/s. This degraded stability can be seen in Figure 5.6, where the capsize mode remains stable with the damping increasing with speed (due to its stability, the capsize nomenclature may seem inappropriate in this case). In contrast, the weave mode is unstable for speeds below 16.4 m/s and the imaginary part is less than 1.4 rad/s. Klein and Sommerfeld attribute the stabilizing effect of front-wheel precession to a self-steering effect; as soon as a bicycle with spinning wheels begins to roll, the resulting gyroscopic moment due to the front wheel part of the $uC_{21}\dot{\varphi}$ term in (5.29) causes the bicycle to steer in the direction of fall. The front contact point consequently takes up a position below the steering assembly mass centre.

The Klein and Sommerfeld findings might leave the impression that gyroscopic effects are essential to auto-stabilization. However, as shown in [191] and discussed in Section 4.4, bicycles without trail or gyroscopic effects can auto-stabilize at modest speeds by adopting extreme mass distributions—but the design choices necessary do not make for a practical vehicle.

5.5 Control-theoretic implications

Locked steering behaviour. As was noted earlier, $P_{11}(s)$ in (5.32) in independent of speed due to the fact that in (5.29) $C_{11} = 0$ and $K_{211} = 0$. This observation is interesting from both a physical and a control theoretic perspective. Suppose the steering degree of freedom is removed. In this case the steering angle $\delta(s)$ must be set to zero in (5.32), and under the assumption of zero external moment T_B, the roll freedom is described by

$$\begin{aligned} 0 &= P_{11}(s)\varphi(s) \\ &= (s^2 I_{Txx} + g m_T z_T)\varphi(s). \end{aligned} \tag{5.35}$$

The roots of $P_{11}(s)$ are given by

$$p_{\pm} = \pm\sqrt{\frac{-g m_T z_T}{I_{Txx}}}, \tag{5.36}$$

where m_T is the total mass of the bicycle and rider, z_T is the height of the combined mass centre above the ground, and I_{Txx} is the roll moment of inertia of the entire machine around the wheelbase ground line. For the data in Table 5.1 $p_{\pm} = \pm 3.1347$.

Since in this case the steering freedom is removed, the A-mode (see Figure 5.5) does not appear. The vehicle's inability to steer also means that the weave mode disappears. Instead, the machine's dynamics are fully determined by the speed-independent, whole-vehicle capsize (inverted-pendulum) mode seen at point B in Figure 5.5 and given by (5.36). Not surprisingly, motorcycles have a tendency to capsize at low speeds if the once-common friction-pad steering is tightened down far enough to lock the steering system; see [192].

5.5.1 A feedback-system perspective

Bicycle as a feedback system. We will now study a steering-related aspect of bicycle behaviour and relate it to the 'locked steering' capsize mode evaluated in (5.36). As Whipple [2] surmised, the rider's main control input is the steering torque. If we suppose the external roll moment is zero, it follows from (5.32) that

$$\varphi(s) = -\frac{P_{12}(s,u)}{P_{11}(s)}\delta(s). \tag{5.37}$$

The second row of (5.32) gives

$$\delta(s) = \frac{-P_{21}(s,u)}{P_{22}(s,u)}\varphi(s) + \frac{1}{P_{22}(s,u)}T_{HB}(s). \tag{5.38}$$

Equations (5.37) and (5.38) are shown diagrammatically in the feedback configuration given in Figure 5.7. Eliminating $\varphi(s)$ yields the closed-loop transfer function

$$H_{\delta T_{HB}}(s,u) = \frac{P_{11}}{\det(P)}(s,u). \tag{5.39}$$

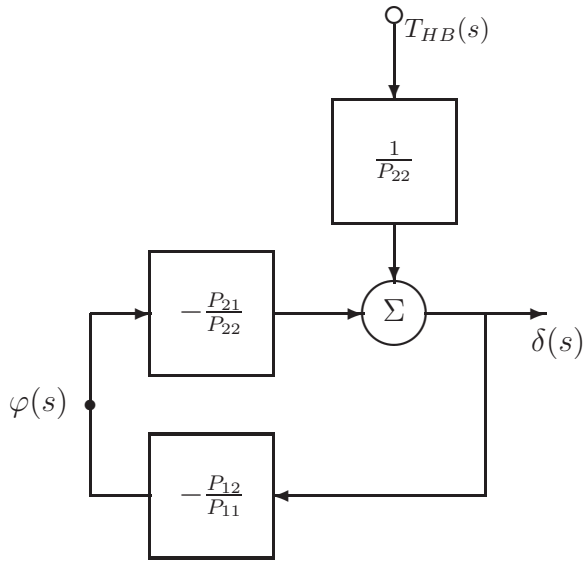

Figure 5.7: Block diagram of the Whipple bicycle model described in (5.32). The steer torque applied to the handlebars is $T_{HB}(s)$, $\varphi(s)$ is the roll angle, and $\delta(s)$ is the steer angle.

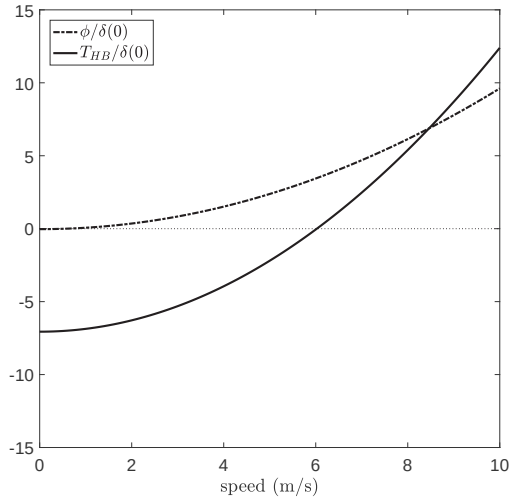

Figure 5.8: Roll angle to steer angle and steer torque to steer angle at equilibrium as a function of speed.

As the speed of the bicycle increases, the unstable poles associated with the static capsize modes coalesce to form the complex pole pair associated with the weave mode. As is clear from Figure 5.5, the weave mode is stable for speeds above 4.3 m/s. For typical datasets $\frac{\phi}{\delta}(0) > 0$; a positive steer angle corresponds to a positive roll angle under steady-state conditions. Also $\frac{\delta}{T_{HB}}(0) < 0$; a positive steer torque corresponds to a negative steer angle under steady-state conditions below the critical capsize speed (6 m/s with the current dataset). Above the critical capsize speed $\frac{\delta}{T_{HB}}(0) > 0$; see Figure 5.8. The zero response in the steer angle (from the steering torque) is due to the singularity of the stiffness matrix $u^2K_2 + gK_0$ at the critical capsize speed.

The poles and zeros of $H_{\delta T_{HB}}(s, u)$, as a function of speed, are shown in Figure 5.9. Save for the pair of speed-independent zeros, this diagram contains the same information as that given in Figure 5.5. The zeros of $H_{\delta T_{HB}}(s, u)$, which derive from the roots of $P_{11}(s)$ as shown in (5.36), are associated with the speed-independent whole-vehicle capsize mode. The backward-running vehicle is seen to be unstable throughout the speed range, but this vehicle is designed for forward motion and, when running backwards, it has negative trail and a divergent castor action.

An explanation for the stabilization difficulties associated with backward-running bicycles centres on the positive zero fixed at $+\sqrt{gm_T z_T / I_{Txx}}$, which is in close proximity to a right-half-plane pole in certain speed ranges [168]. In control terms, this 'almost pole-zero cancellation' in the right-half plane constitutes an unstable 'almost uncontrollable' mode. In the case of an exact cancellation, this unstable uncontrollable mode becomes inaccessible to the rider.

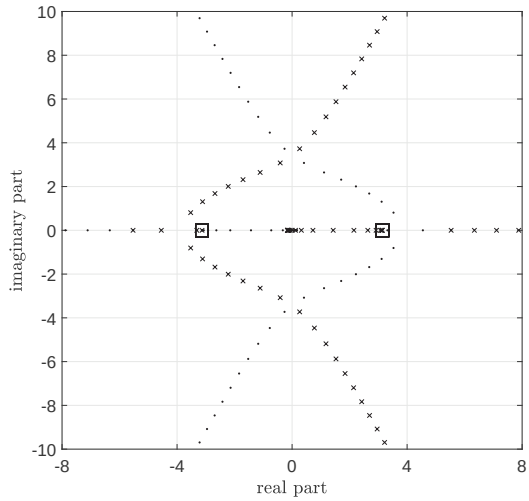

Figure 5.9: Poles and zeros of $H_{\delta T_{HB}}(s, u)$ as functions of speed. The speed u is varied between ± 10 m/s. The poles are shown as dots for forward speeds and crosses for reverse speeds. There are two speed-independent zeros shown as squares at ± 3.1347.

The right-half-plane (positive) zero has fundamental implications for the forward-running vehicle. It is well known that the step response of an asymptotically stable, strictly proper (i.e. more poles than zeros) transfer function exhibits an initial undershoot if the system has an odd number of positive zeros [193]. These systems also tend to be more difficult to control. The steer torque to steer angle transfer function (5.39) is non-minimum phase in the stable speed range. When applying a positive steer torque step, a positive steer angle response results that eventually settles to a negative steady-state value. This negative steady-state steer angle results in a negative steady-state yaw rate (5.26) and a negative roll angle. To summarize, in order to enter a counter-clockwise turn the rider needs to apply a clockwise steer torque. The non-minimum phase zero is the mathematical reason for this counter-steering behaviour.

Steering. The appreciation of the subtle nature of bicycle steering goes back over a hundred years. Archibald Sharp records (p. 222 of [3]) '. . . to avoid an object it is often necessary to steer for a small fraction of a second towards it, then steer away from it; this is probably the most difficult operation the beginner has to master . . . '. While perceptive, such historical accounts make no distinction between steering torque control and steering angle control, they do not highlight the role played by the machine speed [194], and timing estimates are based on subjective impressions, rather than experimental measurement.

We will now examine the role of speed and steering torque in determining the vehicle's trajectory. The steer-torque-to-steer-angle response of the bicycle can be deduced from (5.39). Once the steer angle response is known, the small-perturbation yaw rate response for the model can be found using (5.26), with the lateral displacement then coming from (5.24). It then follows that the transfer function linking the lateral displacement to the steer angle is

$$H_{y_R\delta}(s,u) = \frac{u(u+st)\cos\lambda}{s^2 w}, \tag{5.40}$$

and that the transfer function linking the lateral displacement to the steering torque is given by $H_{y_R T_{HB}} = H_{y_R\delta}(s,u)H_{\delta T_{HB}}(s,u)$, with $H_{\delta T_{HB}}(s,u)$ given in (5.39). This transfer function is used in the computation of responses to steering torque step inputs. The right-half-plane zero in $H_{\delta T_{HB}}(s,u)$ is likely to produce detectable non-minimum phase behaviours.

In order to study the bicycle's steering response at different speeds, including those outside the auto-stable speed range, it is necessary to introduce stabilizing rider control. In this study the rider will be emulated using the roll-angle-plus-roll-rate feedback law

$$T_{HB}(s) = r(s) + (k_\varphi + sk_{\dot\varphi})\varphi(s), \tag{5.41}$$

in which $r(s)$ is a reference torque input, and k_φ and $k_{\dot\varphi}$ are the roll and roll-rate feedback gains respectively. This feedback law can be combined with

$$H_{\varphi T_{HB}}(s,u) = -\frac{P_{12}}{\det P}(s,u)$$

to obtain the open-loop stabilizing steer-torque pre-filter

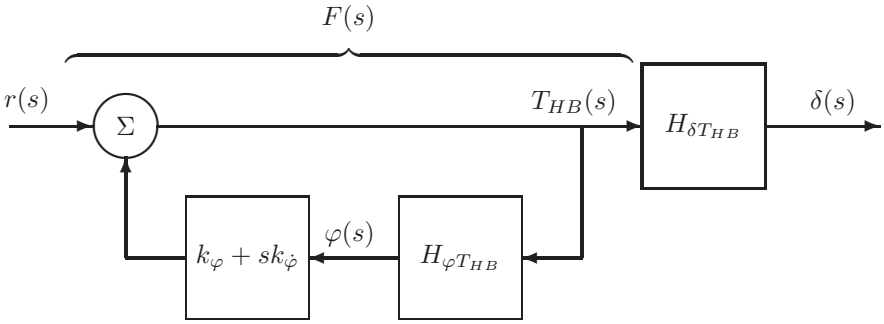

Figure 5.10: Steering torque pre-filter $F(s)$ described in (5.42). This filter is an open-loop realization of the roll-angle-plus-roll-rate feedback law described in (5.41). As readers familiar with control systems will realize, open- and closed-loop systems can be represented in equivalent ways if there are no disturbances and no modelling uncertainties.

$$F(s) = \frac{\det(P(s,u))}{\det(P(s,u)) + (k_\varphi + sk_{\dot\varphi})P_{12}(s,u)}, \tag{5.42}$$

which maps the reference input $r(s)$ into the 'rider-produced' steering torque $T_{HB}(s)$ as shown in Figure 5.10. In the auto-stable speed range the stabilizing pre-filter is not needed and $F(s)$ can be set to unity in this case. The bicycle's steering behaviour can now be studied at speeds below, within, and above the auto-stable speed range. Prior to manoeuvring, the machine is in a constant-speed straight-running trim condition. In each of the three cases, the filtered steering torque, the roll angle, the steering angle, and the lateral displacement responses to a steering torque reference input $r(s)$ are shown in Figure 5.11. The magnitude of the torque step is $r = \varphi_0 \left(\frac{T_{HB}}{\varphi}(0) + k_\varphi\right)$, which is easily verified to give the same steady-state target roll angle φ_0.

The auto-stable case is considered first. In this case the clockwise (when viewed from above) steer torque reference is applied directly to the bicycle's steering system (see Figure 5.11). Following the steer torque input, the bicycle immediately rolls to the left (negative ϕ) in preparation for a left-hand turn. The machine initially steers to the right (positive δ) and the rear-wheel ground-contact point starts moving to the right (positive y_R). After approximately 0.6 s, the steer angle sign reverses, while the rear-wheel ground-contact point begins moving to the left after approximately 1.1 s. In order to turn to the left, one must steer to the right so as the make the machine roll to the left. This property of the machine to apparently roll in the wrong direction is sometimes referred to as 'counter-steering' [188, 195]. The non-minimum phase behaviour in the steer angle and lateral displacement responses is attributable to the right-half-plane zero in $H_{\delta T_{HB}}(s,u)$ given by the roots of $P_{11}(s) = 0$ and corresponding to the locked-steering whole-machine capsize mode as illustrated in (5.36). Towards the end of the simulation shown, the steer angle settles into an equilibrium condition, in which the

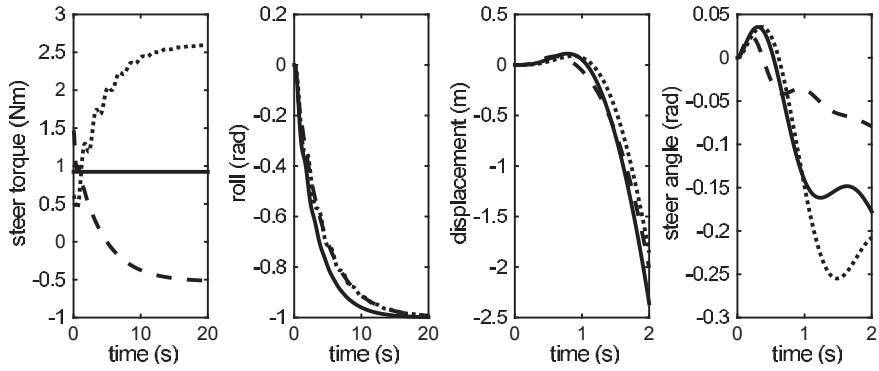

Figure 5.11: Response of the controlled Whipple bicycle to a steering torque reference $r = (T_{HB}/\varphi)(0) + k_\varphi$. The responses at the auto-stable speed of 5 m/s are shown solid; the pre-filter gains are $k_\varphi = k_{\dot\varphi} = 0$. The low-speed 4 m/s case, which is below the auto-stable speed range, is shown dotted; the stabilizing pre-filter gains are $k_\varphi = 2$ and $k_{\dot\varphi} = -1$. The high-speed 7 m/s case, which is above the auto-stable speed range, is shown dashed; the stabilizing pre-filter gains are $k_\varphi = -2$ and $k_{\dot\varphi} = -1$.

bicycle turns left in a circle with a fixed negative roll angle. In relation to the non-minimum phase response in the lateral displacement behaviour, the control difficulty arises if one rides near to a curb [195]: to escape, one has to go initially closer to the edge.

At speeds below the auto-stable range, active stabilizing steering must be utilized in order to prevent the machine from toppling over. In the low-speed (4 m/s) case the steer torque illustrated in Figure 5.11 is the step response of the pre-filter, which is the steer torque required to establish a steady turn. The output of the pre-filter, which crudely mimics the rider, is uni-directional apart from the superimposed weave-frequency oscillation required to stabilize the bicycle's unstable weave mode. In the case considered here, the steady-state steer torque is more than twice the auto-stable reference torque required to bring the machine to a steady-state roll angle of -1 rad. The steer angle and lateral displacement responses are similar to those obtained in the auto-stable case. If the trim speed is increased to the upper limit of the auto-stable range (in this case 6.0 m/s; see Figure 5.5), then the steady-state steering torque required to maintain an equilibrium steady-state turn falls to zero; this response is due to the singularity of the stiffness matrix $u^2K_2 + gK_0$ at this speed.

At speeds above the auto-stable range, stabilizing rider intervention is again required. The interesting variation in this case is in the steering torque behaviour. This torque is initially positive and results in the vehicle rolling to the left. However, if this roll behaviour were left unchecked, the bicycle would topple over, and so to avoid the problem the steer torque immediately reduces and then changes sign after approximately 5 s. The steer torque then approaches a steady-state value of -0.5 Nm in order to stabilize the roll angle and maintain the counter-clockwise turn. This need to steer in one direction to initiate the turning roll angle response, and then to later apply an

opposite steering torque that stabilizes the roll angle, is a high-speed phenomenon, providing an alternative interpretation of the 'counter-steering' phenomenon mentioned earlier. Counter-steering in the non-minimum phase response sense is always present, while in the second sense it is a high-speed[10] phenomenon only.

We will now argue that the pre-filter enforces this type of counter-steering for all stabilizing values of k_φ and $k_{\dot\varphi}$ and not only the particular numerical values chosen. First, the infinite frequency gain of $F(s)$ is unity; this follows from the fact that the numerator and denominator quartic coefficients (in s) are both given by $\det(M)$; see (5.31). Since k_φ and $k_{\dot\varphi}$ are stabilizing, all of the denominator polynomial coefficients of $F(s)$ are positive, as are all of the numerator polynomial coefficients in the auto-stable speed range. As the speed passes from the auto-stable range, $\det(u^2K_2 + gK_0)$ changes sign as does the constant coefficient in the numerator of $F(s)$.[11] Therefore, at speeds above the auto-stable range, $F(s)$ has a negative steady-state gain thereby enforcing the sign reversal in the steering torque as observed in Figure 5.11.

We conclude this section by associating the Whipple bicycle's non-minimum phase response (in the steer angle) with its self-steering characteristics. To do this consider removing the bicycle's ability to self-steer by setting $\alpha = \pi/2$, $t = 0$, $I_{Axz} = 0$, $I_{Fyy} = 0$, and $x_H = w$. With these changes in place, it is easy to check that $P_{21}(s, u) = 0$, which means that (5.38) reduces to

$$\begin{aligned} H_{\delta T_{HB}} &= \frac{1}{P_{22}(s,u)} \\ &= \frac{1}{sI_{Azz}(s + u/w)}, \end{aligned} \tag{5.43}$$

which is clearly minimum phase and represents the response one would expect when applying a torque to the steering assembly inertia in parallel with a speed-dependent 'steering damper'. The damping term is clearly speed-dependent and is related to the rear-wheel rolling constraints.

5.6 Model extensions

5.6.1 Acceleration

The simple model given in (5.29) can be extended to include the effects of acceleration and braking. This extended model takes the form

$$M\ddot{\boldsymbol{q}} + uC\dot{\boldsymbol{q}} + (gK_0 + a_xK_1 + uK_2)\boldsymbol{q} = \begin{bmatrix} T_B \\ T_{HB} \end{bmatrix}, \tag{5.44}$$

in which the stiffness matrix K_1 introduces the effects of an acceleration a_x in the bicycle's longitudinal direction.

We begin from the in-plane dynamics, which are decoupled from the out-of-plane dynamics under the small-perturbation conditions; see Section 5.2.1. Force balance in

[10] In this instance we are referring to speeds above the capsize critical speed—if there is one.

[11] Suppose that $\det(P(s,u)) = \sum_{i=0}^{4} s^i a_i$, then $a_0 = \det(u^2K_2 + gK_0)$, with $P(s,u)$ given by (5.31).

the longitudinal and vertical directions, and a moment balance with respect to the bicycle's mass centre, give

$$0 = F_{x_R} + F_{x_F} - m_T a_x \tag{5.45}$$
$$0 = N_R + N_F - m_T g \tag{5.46}$$
$$0 = -z_T \left(F_{x_R} + F_{x_F}\right) - x_T N_R + (w - x_T) N_F - I_{Ryy}\ddot{\theta}_R - I_{Fyy}\ddot{\theta}_F. \tag{5.47}$$

Solving these equations for the normal loads N_R and N_F, the total longitudinal force $F_{x_R} + F_{x_F}$, and introducing the no-slip constraints $\ddot{\theta}_R = -a_x/r_R$ and $\ddot{\theta}_F = -a_x/r_F$ gives

$$N_R = m_T g \frac{w - x_T}{w} + \Delta N \tag{5.48}$$
$$N_F = m_T g \frac{x_T}{w} - \Delta N \tag{5.49}$$
$$F_{x_R} + F_{x_F} = m_T a_x, \tag{5.50}$$

where

$$\Delta N = -\frac{a_x S_X}{w} \qquad S_X = m_T z_T - \frac{I_{Ryy}}{r_R} - \frac{I_{Fyy}}{r_F}. \tag{5.51}$$

We are now ready to deal with the out-of-plane dynamics. As a result of the bicycle's acceleration, the yaw acceleration and lateral acceleration expressions given in (5.27) and (5.28) must be augmented by the additional acceleration-related terms

$$\Delta\ddot{\psi} = \frac{a_x \delta \cos\lambda}{w} \qquad \text{and} \qquad \Delta\ddot{y}_R = a_x \psi. \tag{5.52}$$

We must also recognize the front-wheel ground-contact longitudinal force F_{x_F}, which accelerates the front wheel. This is computed from the moment equilibrium with respect to the front-wheel centre in (5.8):

$$F_{x_F} = -\frac{S_F}{r_F} a_x \tag{5.53}$$

in which S_F is given by (5.19).

We can now find the acceleration-related terms resulting from (5.51), (5.52), and (5.53) in the roll moment equation (5.21). The change in the front-wheel load, the change in the yaw angle acceleration, the change in the lateral acceleration, and the effect of the lateral (relative to the rear frame) component of F_{x_F} combine to introduce the following additional terms on the left-hand side of the roll balance equation (5.21):

$$\Delta T_R = a_x \delta \left[-\mu S_X + (I_{Txz}/w + S_F)\cos\lambda\right]. \tag{5.54}$$

The yaw moment balance equation (5.22) also requires additional terms when the bicycle is accelerating. Changes in the yaw acceleration, the d'Alembert force on the

front frame assembly, and the yaw-related effect of F_{x_F} must all be recognized. The combined effect of these influences is:

$$\Delta T_Y = \left[a_x \left(\frac{I_{Tzz}}{w} \cos\lambda - m_A u_A - S_F \sin\lambda \right) - F_{x_F}(w+t)\cos\lambda \right] \delta + a_x S_X \varphi. \quad (5.55)$$

Finally, the steer moment balance equation (5.23) must be modified to recognize acceleration-related forces. The combined influence of changes in the the yaw acceleration, changes in the front-wheel normal load, and the d'Alembert force acting on the front frame assembly result in the following change in the steer moment expression:

$$\Delta T_S = a_x \delta \left[\frac{I_{A\lambda z}}{w} \cos\lambda - m_A u_A \cos\lambda - \mu S_X \sin\lambda \right] - \mu a_x S_X \varphi. \quad (5.56)$$

Equations (5.54), (5.55), and (5.56) can be combined to produce the acceleration-related K_1 matrix given in (5.44) above. The first row of K_1 comes from (5.54), while the second row of K_1 is computed using $\mu(5.55) + (5.56)$.

The four entries of the K_1 matrix are

$$\begin{aligned}
K_1(1,1) &= 0 \\
K_1(1,2) &= -\mu S_X + (I_{Txz}/w + S_F)\cos(\lambda) \\
K_1(2,1) &= 0 \\
K_1(2,2) &= -\mu S_X \sin(\lambda) - m_A u_A \mu + ((\mu I_{Tzz} + I_{A\lambda z})/w \\
&\quad + S_F \mu (w + t - r_F \tan\lambda)/r_F - m_A u_A)\cos(\lambda).
\end{aligned}$$

In order to study the machine's behaviour for small perturbations from a straight-running accelerating trajectory, equation (5.44) can be solved numerically. Under accelerating conditions the machine's speed varies and so equation (5.44) is linear-time-varying, because uC and u^2K_2 are time-varying. There is no background 'equilibrium' and the time-varying roots of the associated characteristic equation must be interpreted with care. As is well known from the linear system theory literature, the (frozen-time) eigenvalue–eigenvector pairs do not represent 'modes', and they do not necessarily determine the system's stability either. See [160, 196] and the references therein for further details.

5.6.2 Frame flexibility

A phenomenon known variously as 'speedman's wobble', 'speed wobble', or 'death wobble' is well known to cyclists [197,198]. As the name suggests, wobble is a steering oscillation, not dissimilar to the shimmy oscillations that occur with supermarket trolley wheels, aircraft nose wheels, and in automobile steering systems. Documented records of this phenomenon in bicycles is sparse, but a survey suggested that shimmy at speeds between 4.5 and 9 m/s is unpleasant, while shimmy at speeds between 9 and 14 m/s is dangerous [198]. This study also suggested a wide spread of frequencies for these oscillations. with the most common being between 5 and 10 Hz. Experimental data for bicycle shimmy are reported in [85] and [86]. The first reports frequencies of approximately 7 Hz and speeds of approximately 5 m/s, while the latter reports

frequencies of approximately 7 Hz and speeds in the range 10–17 m/s. The rotational frequency of the front wheel is sometimes close to the wobble frequency, so that forcing from wheel or tyre non-uniformity may be an added influence.

Rough surfaces may break the regularity of the wobble phenomenon thereby eliminating it, but an initial event is normally needed to trigger the problem. Shimmy usually appears during 'hands-off' riding, since the passive damping introduced by the rider is sufficient to damp the oscillations. These stabilizing effects have been reproduced theoretically [199, 200]. Hand-on shimmy is possible in extreme cases. Juden [198] advises: 'pressing one or both legs against the frame, while applying the rear brake' as a helpful practical procedure, if a wobble should commence. The possibility of accelerating out of a wobble is mentioned, suggesting the existence of a worst-case speed. The influences of loading are discussed, with special emphasis on the loading of steering-frame-mounted panniers. Sloppy wheel or steering head bearings and flexible wheels are thought to be contributory.

In an important paper from a practical viewpoint, Wilson-Jones [192] implies that wobble was a common motorcycling phenomenon in the 1950s. Machines of the period were usually fitted with a rider-adjustable friction-pad steering damper. The idea was that the rider should make the damper effective for high-speed running and ineffective for lower speeds; see also [201, 202]. Wilson-Jones offers the view that steering dampers should not be necessary for speeds under 45 m/s, indicating that, historically, wobble in motorcycles has been a high-speed problem. He also points to the dangers of returning from high speed to low speed, while forgetting to lower the preload on the steering damper.

The basic Whipple bike model cannot reproduce lightly damped and possibly unstable shimmy/wobble oscillations. In order to introduce these dynamics into the model, representing the flexible frame and/or the non-instantaneous tyre response is necessary; quantitatively accurate results require both. In this section we deal with the frame flexibility, while the tyre effect will be discussed in Section 5.6.3.

We will now introduce into the Whipple bicycle model a torsional frame flexibility that is perpendicular to the steering axis; see Figure 4.17. This lumped flexibility is used to represent the torsional compliance of the frame and the lateral compliance of the front fork. For the purposes of an initial study, the frame flexibility has been set at 2000 Nm/rad, at a distance 0.922 m from the front contact point, giving a lateral stiffness at the contact point of 2355 N/m. We have also introduced a structural damping of 20 Nm s/rad that acts in parallel with the string. The other data are again from Table 5.1. The eigenvalues of the straight-running linearized Whipple bicycle with frame flexibility are shown in Figure 5.12. As we would now expect, flexibility in the frame has introduced a new shimmy-related mode that is usually referred to as 'wobble'. When comparing Figures 5.12 and 5.5, we observe that the capsize and castor modes remain essentially unaltered. The weave-mode frequency range remains much as it did in the basic Whipple machine, although frame flexibility has a speed-dependent influence on the damping of the weave mode. At low speeds, frame flexibility has no effect, but at intermediate and high speeds the weave mode damping is compromised by the flexible frame, although this mode remains well damped. The wobble mode is new and attributable to frame flexibility. At low speeds this mode

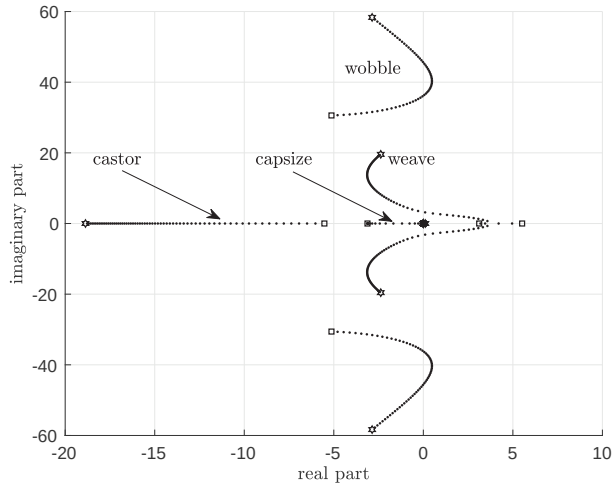

Figure 5.12: Stability properties of the Whipple bicycle with a flexible frame. The speed is varied from 0 to 20 m/s; the zero-speed end is represented by a square and the high-speed end by a hexagram. The torsional stiffness of the frame is 2000 Nm/rad and the frame's damping is 20 Nms/rad.

is well damped with a frequency just below 5 Hz. As the speed increases, the wobble mode frequency increases and its damping reduces until becoming unstable over an intermediate range of speeds, where the modal frequency is approximately 6.5 Hz. At higher speeds approaching 20 m/s the wobble mode frequency continues to increase as does its damping. This calculation has illustrated the possibility that bicycles can have a potentially dangerous wobble mode in the 6–8 Hz range at intermediate speeds.

5.6.3 Pneumatic tyres

There have been many studies into the influence of tyre characteristics on vehicular wheel shimmy; see in Section 3.1. Pacejka's PhD work [92] made an important contribution to the understanding of shimmy in general, concentrating particularly on the automotive context. Pacejka draws a distinction between 'gyroscopic shimmy', occurring in automobiles with beam axle suspensions, which was historically important in influencing the introduction of independent front suspensions for cars, and what he calls 'tyre shimmy' in which gyroscopic effects are not significant. In this latter case, the compliance of the tyre's carcass, together with the relatively high frequency of the oscillations, combine to introduce phase lags between wheel steering motions and tyre lateral forces and aligning moments, which affect the system stability markedly, as control engineers would appreciate. Pacejka drew attention to wheel-bearing clearance and kingpin friction as nonlinear influences on the small-amplitude behaviour, and tyre force saturation as determining the high-amplitude (limit-cycle) behaviour. Prior to Pacejka's research, tyre shimmy had been studied seriously only in an aeronautical

context. Shimmy vibrations using an essential model were simulated and discussed in Section 4.5.

Up to this point in our study of the Whipple bicycle we have modelled the road–tyre rolling contact using velocity (non-holonomic) constraints. This approach is valid at low speeds, but becomes less reliable as the speed increases. Our focus in this section is to replace the road–tyre constraint model employed so far with the small-perturbation force-generating tyre representation of the kind introduced in Sections 3.7 and 3.8. A single-point-contact model is employed, where the lateral force response of the tyre due to steering, and therefore side slipping, is a dynamic response to the slip and camber angles of the tyre, which is modelled with a first-order relaxation equation as

$$\sigma \frac{dF_y}{ds} + F_y = F_z(C_\alpha \alpha + C_\varphi \varphi), \tag{5.57}$$

where σ is the relaxation length, F_z is the tyre normal load, α is the side-slip angle, and φ is the wheel's camber angle relative to the road. This model is used for both wheels, with the tyre parameters given in the following table:

Parameter	Value
$C_{\alpha r}$	14.0
$C_{\alpha f}$	14.0
$C_{\varphi r}$	1.0
$C_{\varphi f}$	1.0
σ_r	0.1 m
σ_f	0.1 m

The subscripts r and f are used to denote 'rear' and 'front' respectively. The products $C_{r/f1} = F_z C_{\alpha r/f}$ are the tyres' cornering stiffnesses, while the products $C_{r/f2} = F_z C_{\varphi r/f}$ are the tyres' camber stiffnesses.[12] It is now shown that the force-generating tyre model has a strong impact on the predicted properties of both wobble and weave.

[12] The following free body diagram represents an inverted-pendulum-type lumped-mass model of a bicycle under steady cornering:

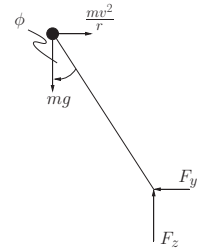

The forces acting on the bicycle's mass centre are the gravitational force mg and the centripetal force $\frac{mv^2}{r}$. Under equilibrium conditions the normal load is $F_z = mg$, while the tyre side force is $F_y = \frac{mv^2}{r}$. In the case of non-dissipative rolling the side-slip is zero and there is no corresponding side-slip-generated side force. Since

$$\frac{v^2}{rg} = \tan\phi \approx \phi$$

for small roll angles, and $F_y = F_z C_{\varphi r/f}\phi$, we conclude that under these conditions $C_{\varphi r/f} = 1.0$.

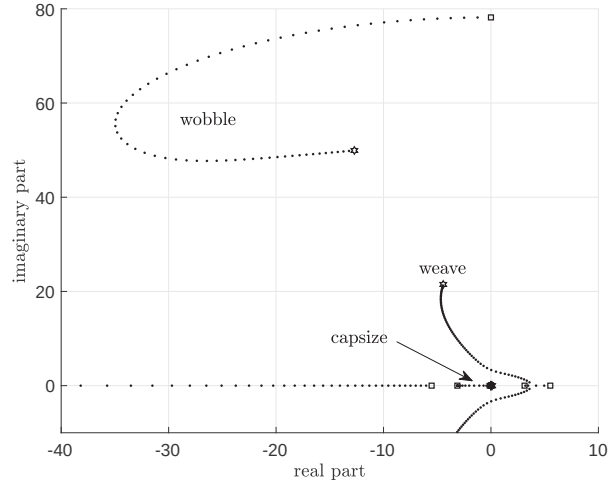

Figure 5.13: Stability properties of the Whipple bicycle with relaxed side-slipping tyres. The speed is varied from 0 to 20 m/s; the zero-speed end is represented by a square and the high-speed end by a hexagram.

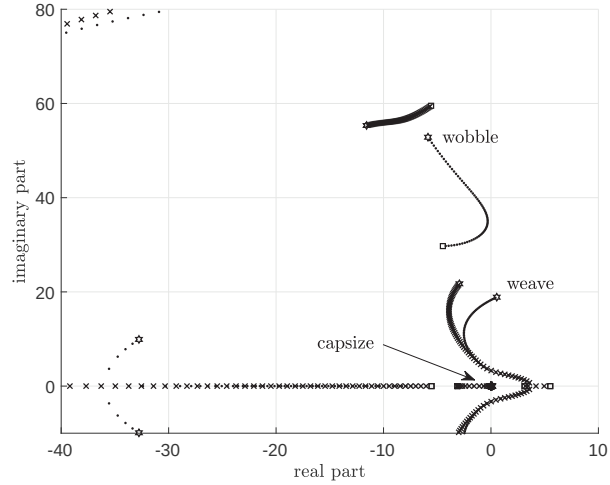

Figure 5.14: Stability properties of the Whipple bicycle with relaxed side-slipping tyres and a flexible frame. The speed is varied from 0 to 20 m/s; the zero-speed end is represented by a square and the high-speed end by a hexagram. The crossed loci represent a stiff-framed machine, while the dotted loci represent a more flexible vehicle. The properties illustrated here for the limited speed range of the bicycle are remarkably similar to those of the motorcycle, with its extended speed capabilities.

As can be seen in Figure 5.13, the introduction of side-slipping tyres also produces a wobble mode, which is not present in Figure 5.5. The resonant frequency of the very low-speed wobble mode is approximately 12.7 Hz, with low predicted damping. As the speed increases, the wobble mode frequency drops to approximately 8.0 Hz. The associated damping increases with speed and then reduces again as the machine speed approaches the top illustrated speed of 20 m/s. As with the flexible frame, side-slipping tyres have little impact on the weave mode at low speeds. However, as the speed increases, the relaxed side-slipping tyres cause a significant reduction in the intermediate and high-speed weave-mode damping.

Figure 5.14 illustrates the influence of a flexible frame in combination with relaxed side-slipping tyres; the characteristics of both stiff and more flexible (stiffness halved) vehicles are illustrated. This figure shows that the introduction of side-slipping tyres causes a reduction in the wobble-mode frequency range. As the frame stiffness increases, this effect becomes more and more pronounced. By extension from measured motorcycle behaviour, there is every reason to suspect that the accurate reproduction of bicycle wobble-mode behaviour requires a model that includes both relaxed side-slipping tyres and flexible frame representations.